Supporting Information

Unlocking Superior Li^+ Transport and Anodic Compatibility for Solid Polymer Electrolytes by Zwitterionic Metal–Organic Filler–Mediated Li^+ Coordination Engineering

Mochun Zhang,‡[a] Zhengguang Li,‡[b] Yuyan Liu,[c] Bo Hong,[a,d,e,f,g] Fuhua Yang,[a,d,e,f,g] Mengran Wang,*[a,d,e,f,g] Die Liu,*[b] Pingshan Wang,[b] Yanqing Lai*[a,d,e,f,g,h]

a School of Metallurgy and Environment, Central South University, Changsha 410083, P. R. China
b Department of Organic and Polymer Chemistry, Hunan Key Laboratory of Micro & Nano Materials Interface Science, College of Chemistry and Chemical Engineering, Central South University, Changsha 410083 P. R. China
c College of Chemistry, Nankai University, Tianjin 300071, P. R. China
d Engineering Research Centre of Advanced Battery Materials, The Ministry of Education, Changsha 410083, P. R. China
e National Energy Metal Resources and New Materials Key Laboratory, Changsha 410083, P. R. China
f National Engineering Research Center of Advanced Energy Storage Materials, Changsha 410083, P. R. China
g Hunan Provincial Key Laboratory of Nonferrous Value-Added Metallurgy, Changsha 410083, P. R. China
h Yuelushan Center for Industrial Innovation, Changsha 410083, P. R. China

* Corresponding author
Email addresses: mengranwang93@163.com (Mengran Wang), chem-ld@csu.edu.cn (Die Liu), laiyanqing@csu.edu.cn (Yanqing Lai)

1.Experimental section

Materials

Poly(vinylidene fluoride-co-hexafluoropropylene) (PVDF-HFP, average Mw: ~400,000), N, N-Dimethylformamide (DMF, >99.9%), Lithium hydroxide (LiOH, 99.9%), 5-aminosalicylic acid (≥98%), boric acid (99.99%), Acetonitrile (ACN) were all purchased from Shanghai Macklin Biochemical Technology Co., Ltd. 1,3,5-tris(bromomethyl)-2,4,6-trimethylbenzene (≥98%), 4-bromo-2-hydroxybenzaldehyde (≥98%), 4-formylphenylboronic acid (≥98%) and 2-acetyl-4-methylpyridine were purchased from Bidepharm (Shanghai, China). lithium bis(trifluoromethanesulfonyl)imide (LiTFSI, 99.9%) was procured from Duoduochem without further purification. Carbon black and PVDF (99.5%) were obtained from Taiyuan Liyuan Lithium Technology Center. $LiNi_{0.8}Co_{0.1}Mn_{0.1}O_2$ (NCM811) powder was sourced from the Minmetals New Energy Materials (Hunan) Co., Ltd. All the materials were stored in an Ar-filled glove box (H_2O < 0.1 ppm, O_2 < 0.1 ppm).

Preparation of Cage

To a mixed solvent of $CHCl_3$ (100 mL) and MeOH (100 mL) ligand **L** (306 mg, 0.2 mmol) was added, then a solution of $Zn(NO_3)_2 \cdot 6H_2O$ (89.4 mg, 0.3 mmol) in CH_3OH (10.0 mL) was added. After stirring the mixture at 65 °C for 12 h, excess $Li(NTf)_2$ was added to precipitate the complex, which was then filtered, washed with H_2O, and then dried *in vacuo*. The desired **Cage** was obtained (92%) as the pale-yellow solid.

Preparation of LiB5AB

lithium bis (5-Aminosalicylic acid) borate (LiB5AB) was synthesized according to the procedure described in Figure S2. 0.39 g of Lithium hydroxide (16.5 mmol), 5.00 g of 5-aminosalicylic acid (33 mmol), and 1.01 g of boric acid (16.5 mmol) were added to acetonitrile and heated at 80 °C. A light brown solid powder was collected by filtration. The ^{1}H, ^{11}B NMR, and mass spectra of LiB5AB are shown in Figure S2.

Preparation of LS filler

The cage was dissolved in anhydrous DMF to prepare a dark brown solution with a concentration of 19 mg mL^{-1}. 6 mL of this solution was accurately measured and placed in a glass reaction bottle. Then, 11.1 mg of the LiB5AB was added. The reaction bottle was transferred to a glove box and stirred

at 60 °C for 24 h. During the reaction, it could be observed that LiB5AB was completely dissolved, and the solution color gradually changed from dark brown to yellow, followed by the precipitation of yellow precipitate. After the reaction was completed, the reaction bottle was removed from the glove box, and no washing was required. It was directly subjected to ultrasonic treatment for 30 min, then returned to the glove box for continued stirring overnight. Finally, a uniformly dispersed product LS dispersion liquid was obtained.

Preparation of LSPH and PH-Li electrolytes

In the synthesized LS dispersion solution, 400 mg of PVDF-HFP and 270 mg of LiTFSI were directly added and stirred continuously at room temperature for 12 h to obtain a uniform casting solution. Then, the casting solution was poured into an 18 mm diameter polytetrafluoroethylene (PTFE) mold and the mold was placed on a heating plate. It was dried at 60 °C for 12 h and then at 80 °C for 4 h to finally obtain the LSPH electrolyte membrane. In this formulation, the mass of LS corresponds to approximately 30 wt.% relative to PVDF-HFP.

The preparation process of the PH-Li electrolyte is similar to that of LSPH, but no LS filler is introduced. The specific steps are: measure 6 mL of DMF solvent, add 400 mg of PVDF-HFP and 270 mg of LiTFSI, and stir at room temperature for 12 h to form a uniform solution. The solution was poured into the same PTFE mold and dried at 60°C for 12 h. The key difference from the LSPH process is that this process does not undergo a secondary drying at 80°C to retain a certain amount of residual DMF solvent, thereby obtaining the PH-Li electrolyte membrane.

Materials characterization

In situ Fourier transform infrared spectroscopy (FTIR) was employed to analyze the functional group changes of the electrolytes before and after polymerization, enabling the assessment of polymerization success. FTIR measurements were conducted using a Nicolet iS50 instrument (Thermo Fisher Technology), with an infrared spectral range of 400–4000 cm^{-1}. Both the monomer and the prepared solid electrolyte were tested in a room temperature air atmosphere.

Thermogravimetric analysis (TGA) was used to investigate the thermal stability of the solid electrolytes. The thermal analysis was performed using an STA 449 F5 Jupiter instrument (Nez Instrument Manufacturing, Germany) with a test temperature range of 30–600 °C, a heating rate of 10

°C min^{-1}, and a nitrogen atmosphere.

X-ray diffraction (XRD) was employed to determine the crystallinity of the solid electrolyte. XRD measurements were carried out with a Rui Ying 2Empyrean 2 instrument (PANalytical, Netherlands) using a copper target, with an angle range of 10° to 80° and a sweep speed of 10° min^{-1}.

Scanning electron microscopy (SEM) was used to examine the microstructure of the polymer solid electrolyte and electrode plates. An energy dispersive X-ray spectrometer (EDS) was also employed to investigate the elemental distribution on the surface of materials through point scanning, line scanning, and surface scanning. The SEM instrument used was a TESCAN CLARA model.

Transmission electron microscopy (TEM) was used to observe the ultrastructure of the materials, particularly the active material properties of the recycled lithium cobalt oxide electrode. The TEM measurements were conducted with a JEM-F200 instrument (JEOL, Japan).

X-ray photoelectron spectroscopy (XPS) was used to analyze the chemical states and molecular structures of elements on the material's surface, particularly to examine the composition of the interface layer on the positive and negative electrodes after cycling. The XPS analysis was performed using an ESCALAB 250Xi instrument (Thermo Fisher Scientific).

^{1}H NMR,^{13}C NMR, ^{11}B NMR, ^{19}F NMR, NOESY, COSY and DOSY spectra were recorded on Bruker Avance 400-MHz or 500-MHz NMR spectrometers using $CDCl_3$, d_6-DMSO and CD_3CN as the solvents with tetramethylsilane (TMS) as the internal standard at room temperature. ESI mass spectrometry were conducted on a Waters Synapt HDMS G2-Si instrument with a LockSpray ESI source, using the following parameters: ESI capillary voltage, 1.3-3.0 kV; sample cone voltage, 20-25 V; extraction cone voltage, 1.1-3 V; desolvation gas flow, 800 L/h (N_2); trap collision energy (CE), 4 V; transfer CE, 0 V; trap gas flow, 2.0 mL/min (Ar); source temperature, 30 ℃; and desolvation temperature, 30 ℃. All samples were dissolved in $CH_3CN/CHCl_3$ or CH_3CN/DMF (1:1, v/v). Data were collected and analyzed by using MassLynx 4.2 (Waters).

Electrochemical characterization

The steel symmetric battery was assembled in a glove box, and electrochemical impedance spectroscopy (EIS) was conducted using a Gamry intrument to measure the impedance of the battery. Afterward, the steel symmetric battery was disassembled, and the thickness of the in-situ polymerized solid electrolyte film was measured. The ionic conductivity (σ) of the electrolyte was then calculated

using the following formula:

$$\sigma = \frac{L}{RS}$$

Where the σ represents the ion conductivity of electrolyte, L is the thickness of electrolyte, R is the impedance, and S is the effective area of the electrolyte.

The activation energy is the energy barrier that lithium ions must overcome during internal migration within the battery. The ion conductivity (σ) of different temperatures was fitted into the Arrhenius model to calculate the activation energy (E_a) of PVT, PVT-C and PVT-CB electrolytes. The formula is as follows:

$$\sigma(T) = Aexp(-\frac{E_a}{RT})$$

Where E_a is the activation energy, A is the pre-exponential factor, and R is the ideal gas constant (8.314 J mol^{-1} K^{-1})

The calculation of lithium-ion transference number (t_{Li+}) was determined by assembling lithium symmetric batteries Li|SPEs|Li. Chronoamperometry was performed by applying a constant voltage of 10 mV, and the impedance in the frequency range of 0.1 Hz to 1 MHz was recorded before and after the test. The lithium-ion transference number was calculated using the following formula:

$$t_{Li+} = \frac{I_{SS}(\Delta V - I_0 R_0)}{I_0(\Delta V - I_{SS} R_{SS})}$$

Where ΔV is the polarization voltage, I_0 and I_{SS} represent the initial and steady-state currents, and R_0 and R_{SS} are the interfacial impedances before and after polarization, respectively.

To evaluate the interfacial stability of the electrolytes with the electrodes, batteries based on SS|SPE|Li were tested using linear sweep voltammetry (LSV). The voltage sweep was applied from 3 V to 6 V at a sweep rate of 1 mV s^{-1}.

The galvanostatic charge-discharge performance of the batteries based on Li|SPEs|Li was tested using a LAND battery test system with a current density of 0.1 mA cm^{-2}. Additionally, to evaluate the stripping and deposition behavior of the lithium metal anode, tests were conducted at different current densities. For the Li|SPEs|NCM811 batteries, the cycling stability was assessed with charge and discharge voltages set between 2.5 and 4.5 V, using the same LAND battery test system.

Theoretical Calculations

The calculations about binding energy were carried out using a DFT framework as implemented with the projector augmented wave (PAW) method by the Vienna Ab-initio Simulation Package (VASP).[1, 2] The electronic exchange-correlation interaction was described by the Perdew-Burke-Ernzerhof (PBE) functional under the generalized gradient approximation (GGA).[3] The kinetic cutoff energy for the plane-wave basis was set to 450 eV and the convergence thresholds of total energy and force during geometry optimizations were 10^{-5} eV and 0.03 eV $Å^{-1}$, respectively. Meanwhile, the DFT-D3 method was adopted to take the long-range van der Waals interaction into account.[4] The Brillouin zone was sampled using the Gamma-centered Monkhorst-Pack method with a k-point mesh of 0.04 2π $Å^{-1}$ for geometry optimizations of all configurations.[5] The ab-initio molecular dynamics (AIMD) simulations were conducted at normal pressure and temperature in the canonical ensemble via Nosé-Hoover thermostat for 12ps with the time step 1fs.[6, 7] The plane-wave cutoff energy was reset to 400 eV and the convergence criterion for the electronic steps was reset to 1×10^{-4} eV. Except for LS-cage, the model systems were composed of LiTFSI, DMF, and short-chain PVDF-HFP, with a molar ratio of 1.00:3.44:3.46 and a bulk density of 0.938 g cm^{-3}.

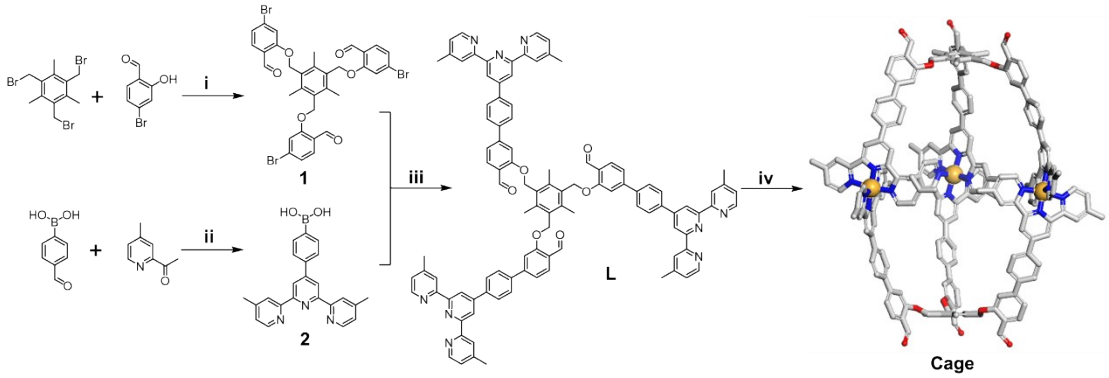

Figure S1 The route for synthesizing ligand **L** and **Cage**. Reagents and conditions: (i) K_2CO_3, DMF, 90°C, 24h; (ii) NaOH, EtOH, $NH_3 \cdot H_2O$; (iii) toluene/H_2O/*t*-BuOH (3:3:1, *v/v/v*), K_2CO_3, $Pd(PPh_3)_4$, refluxed; (iv) $Zn(NO_3) \cdot 6H_2O$, $CHCl_3$/MeOH, refluxed.

Compound 1. 1,3,5-tris(bromomethyl)-2,4,6-trimethylbenzene (3.98 g, 10.0 mmol), 4-bromo-2-hydroxybenzaldehyde (7.24 g, 36.0 mmol) and K_2CO_3 (12.4 g, 90.0 mmol) were added into a 250 mL round-bottomed flask with 100 ml DMF as solvent. After stirring at 90°C for 24 hours, the reaction mixture was cooled to 25°C. The mixture was extracted with $CHCl_3$ and the combined organic extract was evaporated to dryness *in vacuo* to give a reside, then subjected to column chromatography (SiO_2, CH_2Cl_2/MeOH = 100:2) for giving **Compound 1** (6.45 g, 85%); ^{1}H NMR (400 MHz, $CDCl_3$) δ 10.31 (s, 3H), 7.73 (d, J = 8.2 Hz, 3H), 7.39 (s, 3H), 7.25 (d, J = 8.8 Hz, 3H), 5.24 (s, 6H), 2.48 (s, 9H); ^{13}C NMR (100 MHz, $CDCl_3$) δ 188.63, 161.41, 140.11, 130.96, 130.74, 129.83, 124.90, 124.09, 116.40, 66.07, 16.38; ESI/MS (m/z): Calcd. For $[C_{33}H_{27}Br_3O_6+H]^+$: 759.29, Found: 759.54.

Compound 2 was synthesized according to a literature procedure.[8]

Compound L. To a flask containing **Compound 1** (1.52 g, 2 mmol), **Compound 2** (2.74 g, 7.2 mmol) and K_2CO_3 (2.48 g, 18 mmol), a mixed solvent (140 mL) of toluene/H_2O/*t*-BuOH (3:3:1, *v/v/v*) was added. After $Pd(PPh_3)_4$ (346 mg, 0.3 mmol) was added, the system was pumped and backfilled with nitrogen. Then the mixture was refluxed for 2 days under N_2. After cooled to 25°C, the mixture was extracted with $CHCl_3$ and the combined organic extract was evaporated to dryness *in vacuo* to give a reside that was washed with MeOH, then subjected to column chromatography (Al_2O_3, CH_2Cl_2/MeOH = 100:2) and then recrystallized from a mixture of $CHCl_3$/MeOH to give **Compound L**, as a light yellow solid (2.14 g, 70%); ^{1}H NMR (400 MHz, $CDCl_3$) δ 10.45 (s, 3H), 8.76 (s, 6H), 8.59 (d, J = 5.0 Hz, 6H), 8.48 (s, 6H), 8.03 (d, J = 8.0 Hz, 6H), 7.97 (d, J = 8.0 Hz, 3H), 7.80 (d, J = 8.0 Hz, 6H), 7.49 (s, 3H), 7.37 (d, J = 8.0 Hz, 3H), 7.19 (d, J = 5.1 Hz, 6H), 5.41 (s, 6H), 2.59 (s, 9H), 2.52 (s, 18H); ^{13}C NMR (100 MHz, $CDCl_3$) δ 189.36, 161.78, 156.38, 156.03, 149.36, 149.10, 148.41, 148.27, 140.56, 139.98, 138.82, 131.36, 129.11, 128.06, 127.97, 125.07, 124.25, 122.30, 120.32, 118.99, 111.40, 65.95, 21.51, 16.48; ESI/MS (m/z): Calcd. For $[C_{102}H_{81}N_9O_6+H]^+$: 1528.83, Found: 1528.63.

Cage. To a mixed solvent of $CHCl_3$ (100 mL) and MeOH (100 mL) ligand **L** (306 mg, 0.2 mmol) was added, then a solution of $Zn(NO_3)_2 \cdot 6H_2O$ (89.4 mg, 0.3 mmol) in CH_3OH (10.0 mL) was added. After stirring the mixture at 65 °C for 12 h, excess $Li(NTf)_2$ was added to precipitate the complex, which was then filtered, washed with H_2O, and then dried *in vacuo*. The desired **Cage** was obtained (92%)

as the pale-yellow solid. ^{1}H NMR (400 MHz, Acetonitrile-d_3) δ 10.51 (s, 6H), 9.03 (s, 12H), 8.63 (s, 12H), 8.38 (d, J = 8.2 Hz, 12H), 8.22 (d, J = 8.0 Hz, 12H), 8.03 (d, J = 8.0 Hz, 6H), 7.83 (s, 6H), 7.69 (d, J = 5.3 Hz, 12H), 7.63 (d, J = 8.1 Hz, 6H), 7.24 (d, J = 5.2 Hz, 12H), 5.55 (s, 12H), 2.65 (s, 18H), 2.50 (s, 36H).

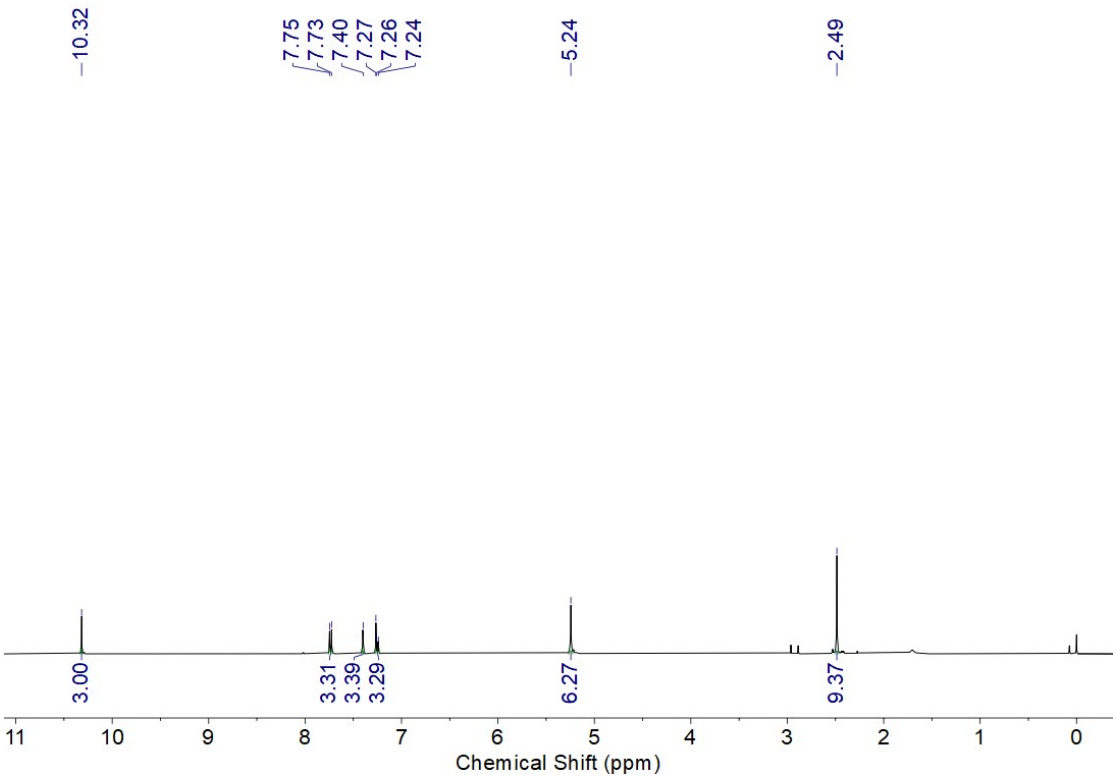

Figure S2. ^{1}H NMR spectrum of **Compound 1** in $CDCl_3$.

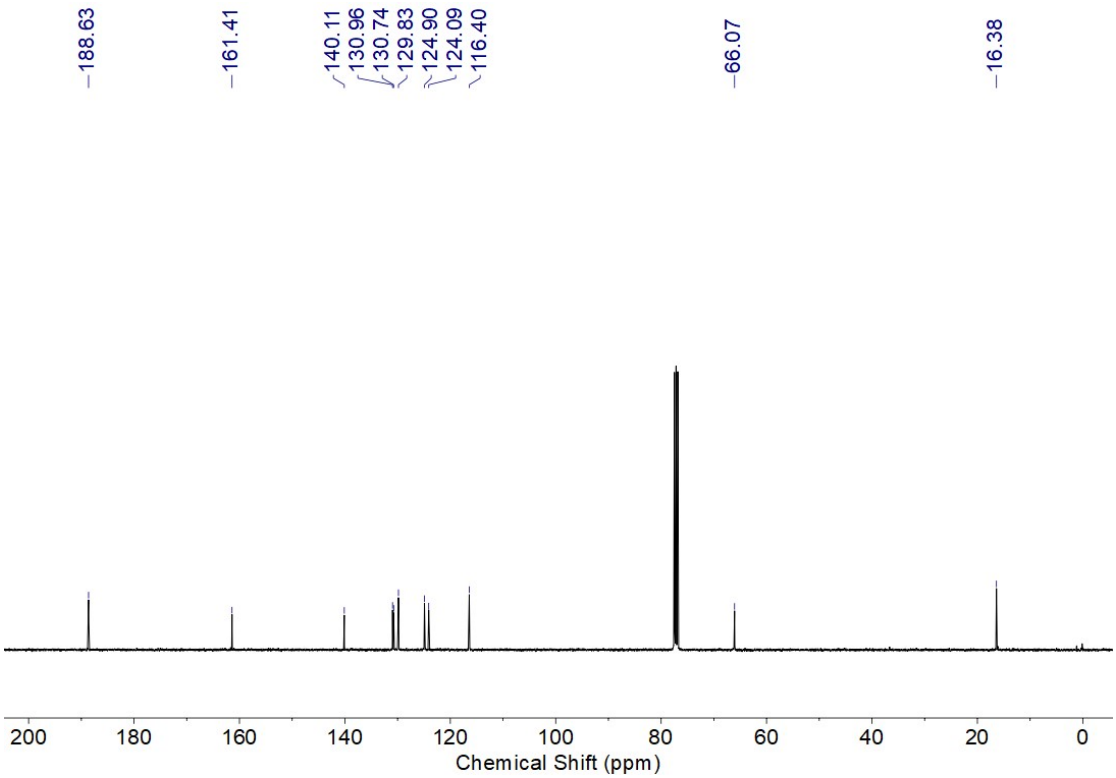

Figure S3. ^{13}C NMR spectrum of **Compound 1** in $CDCl_3$.

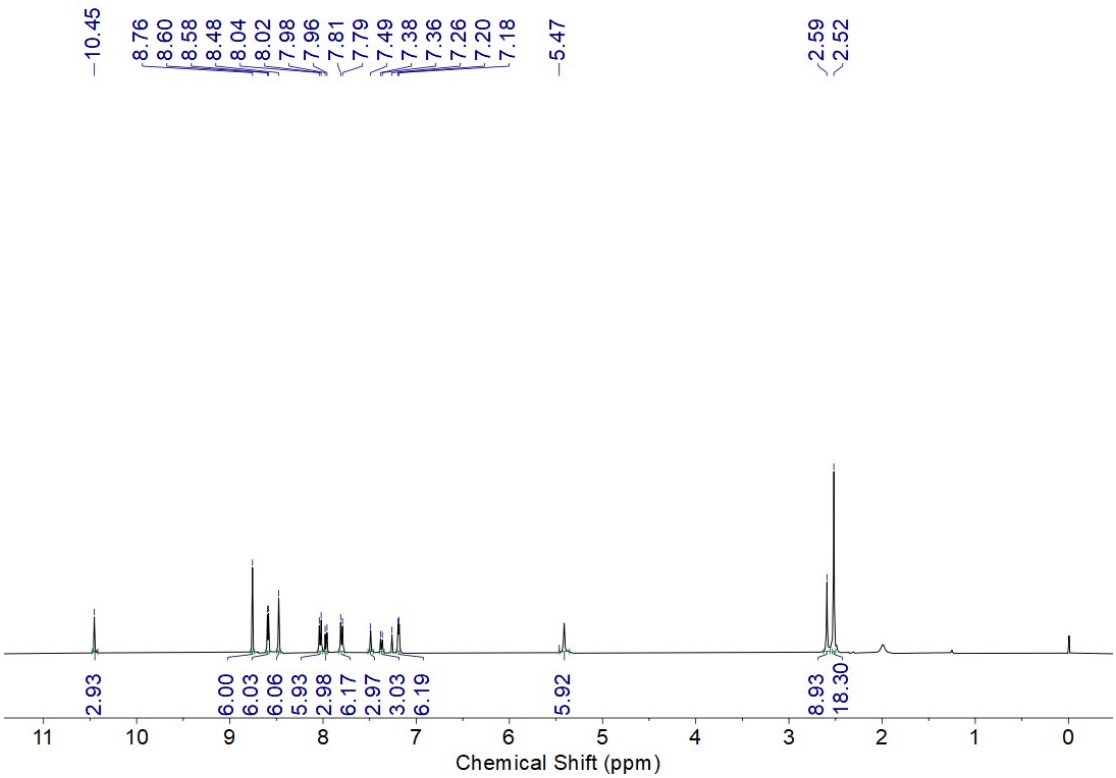

Figure S4. ^{1}H NMR spectrum of **Compound L** in $CDCl_3$.

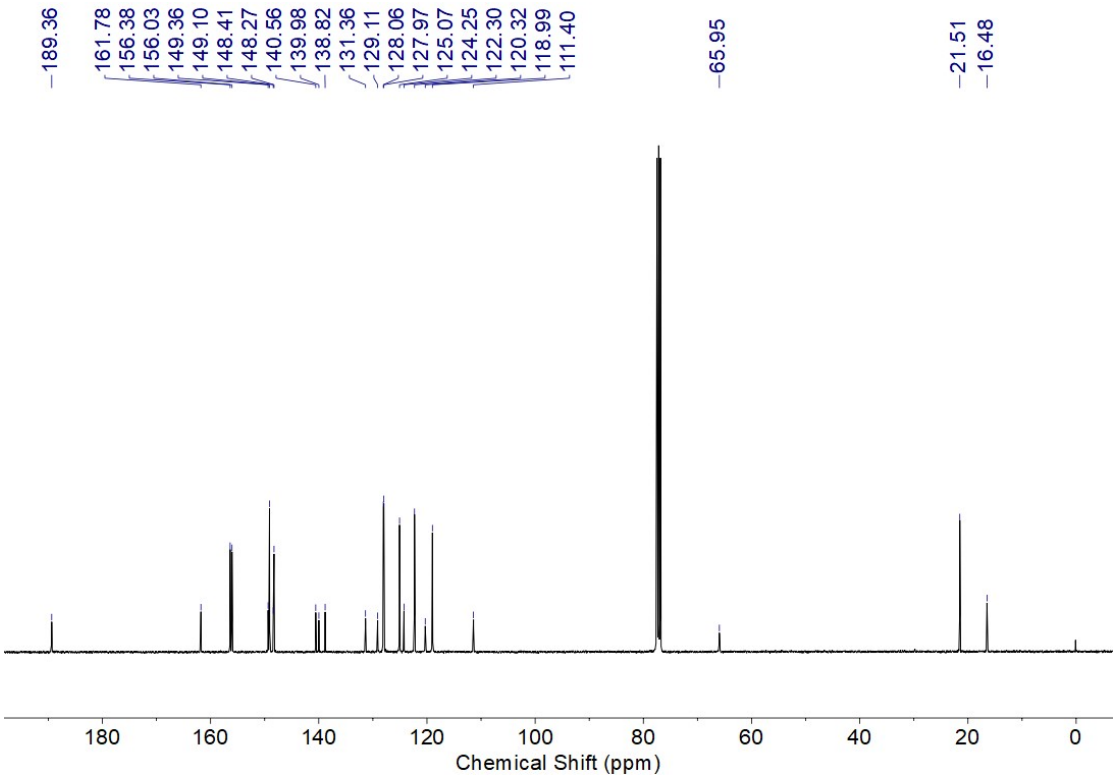

Figure S5. ^{13}C NMR spectrum of **Compound L** in $CDCl_3$.

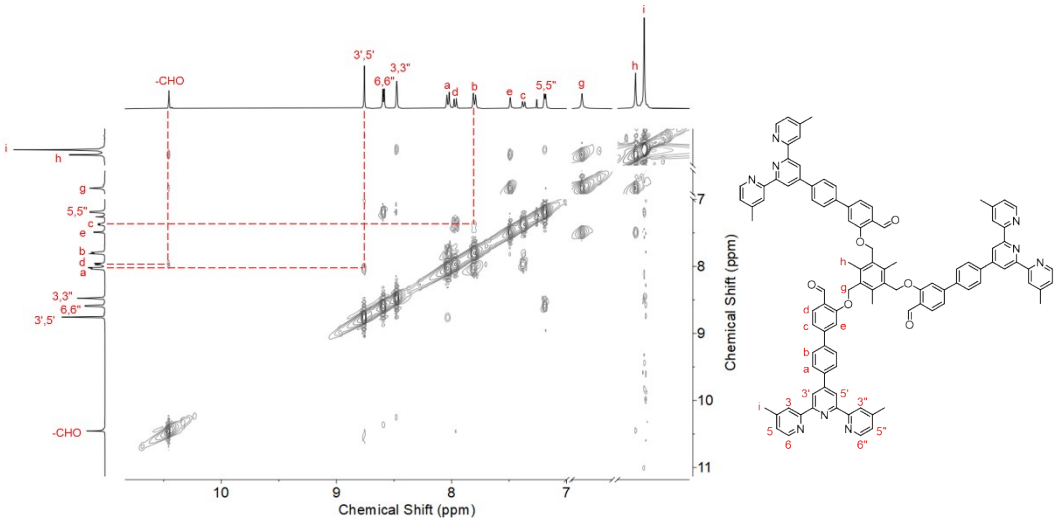

Figure S6. NOESY spectrum of **Compound L** in $CDCl_3$.

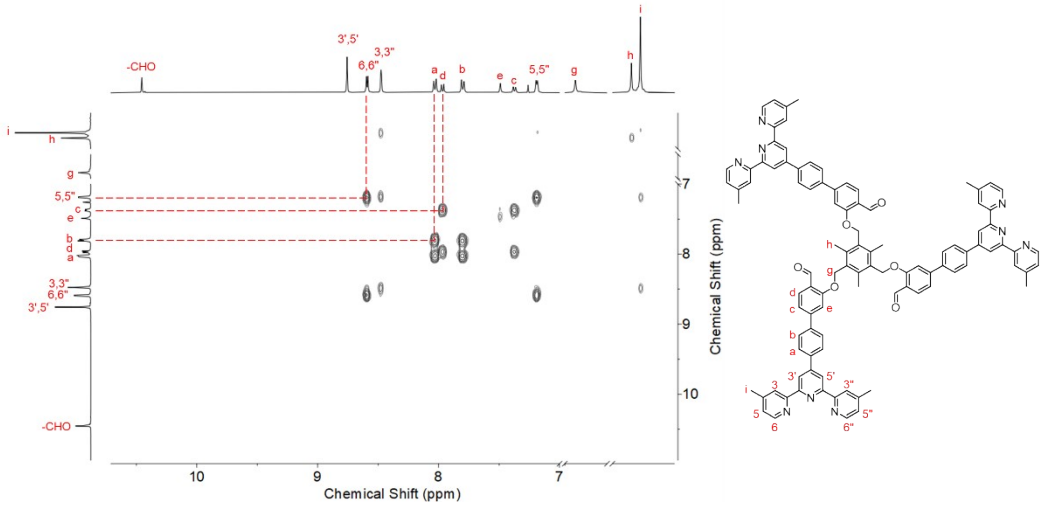

Figure S7. COSY spectrum of **Compound L** in $CDCl_3$.

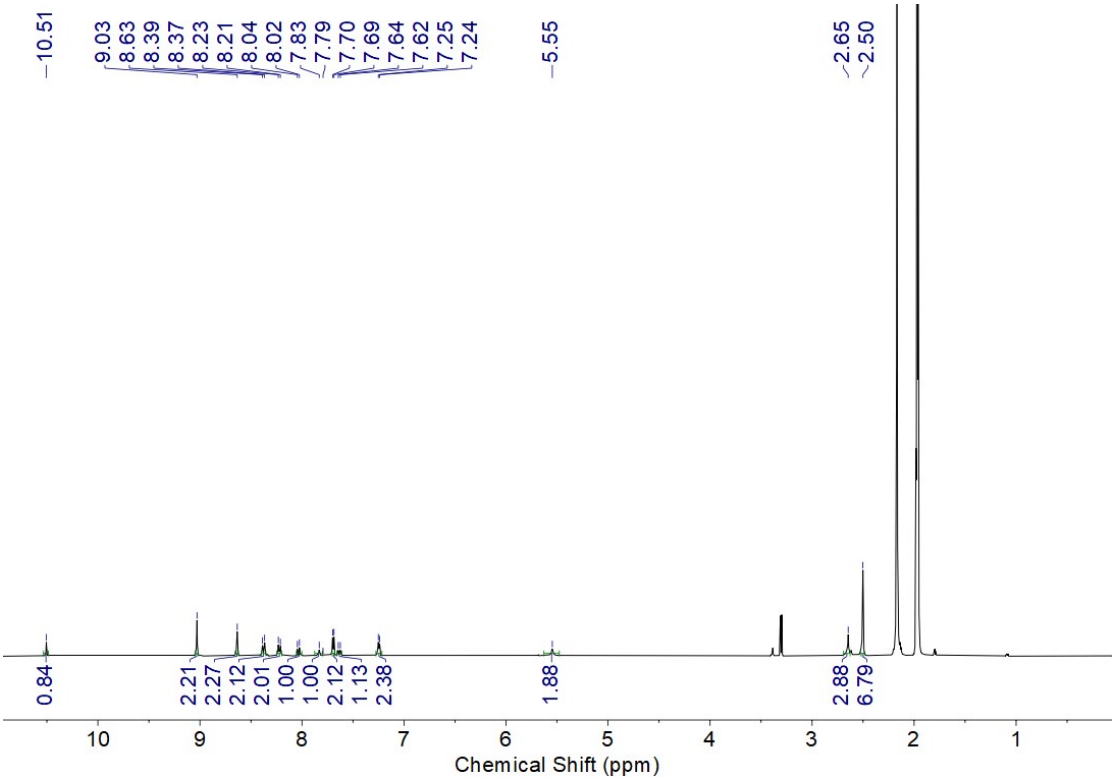

Figure S8. ^{1}H NMR spectrum of **Cage** in CD_3CN.

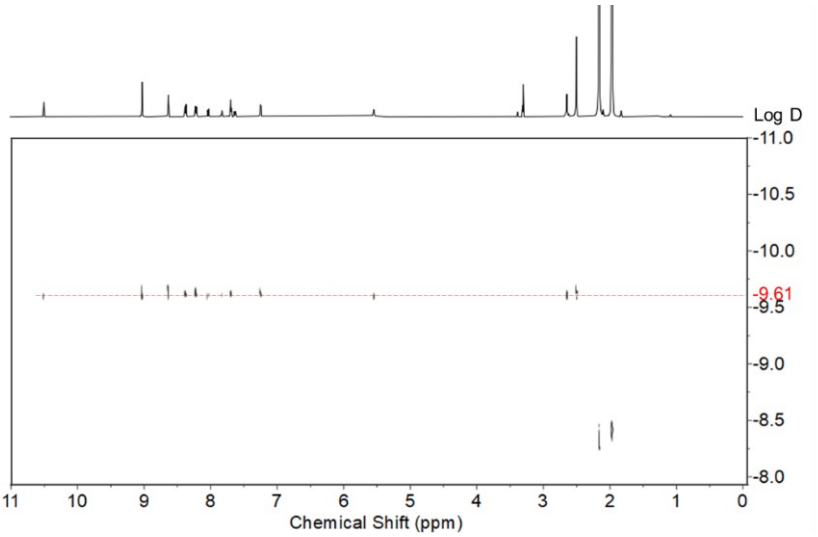

Figure S9. DOSY spectrum of **Cage** in CD_3CN.

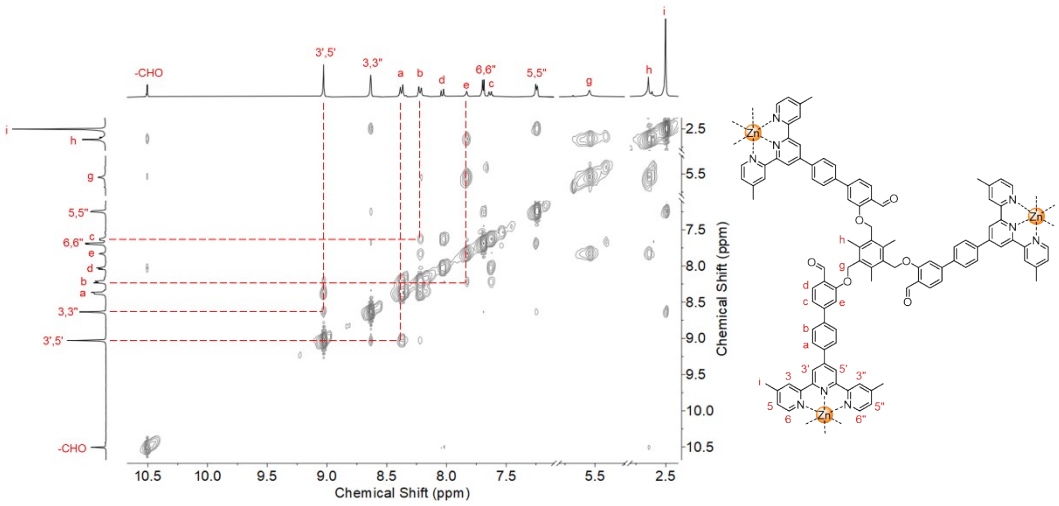

Figure S10. NOESY spectrum of **Cage** in CD_3CN.

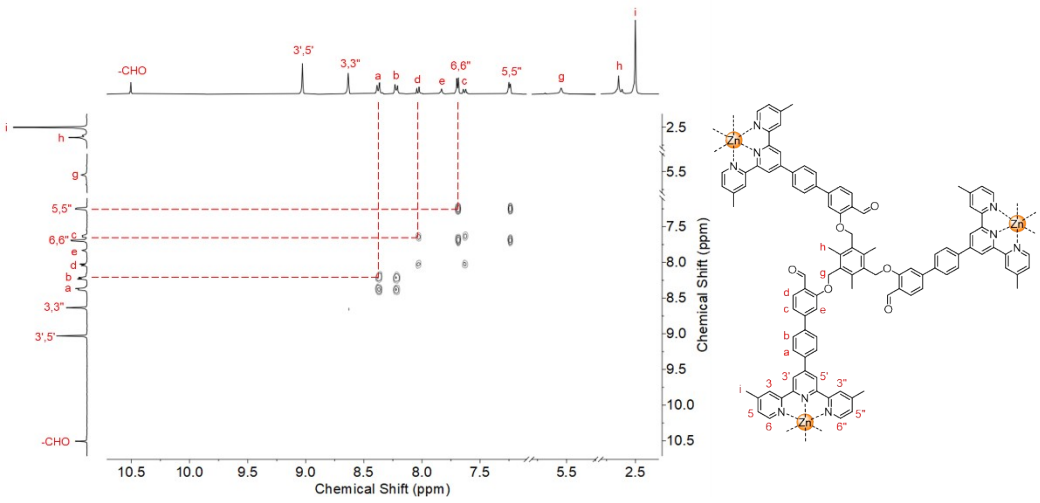

Figure S11. COSY spectrum of **Cage** in CD_3CN.

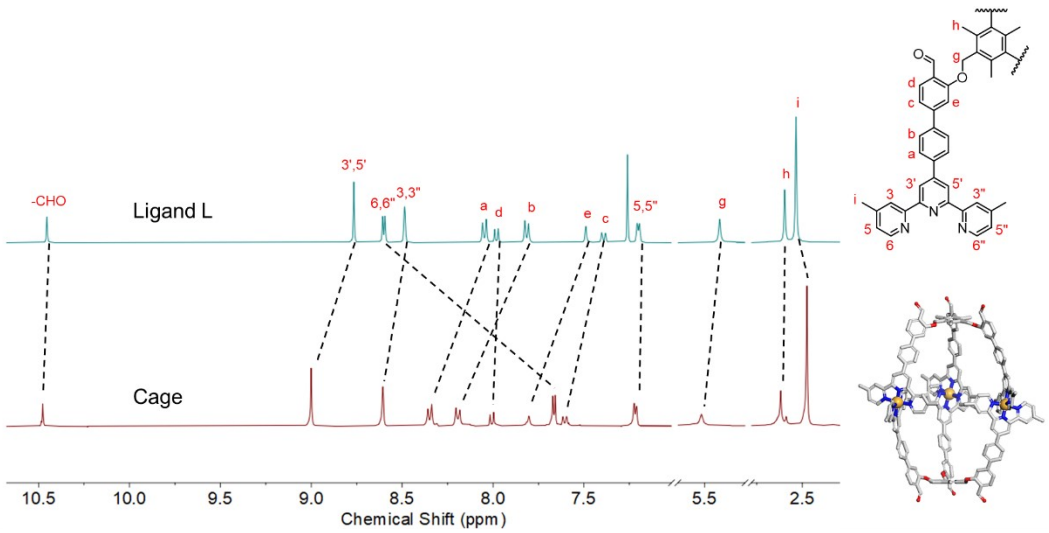

Figure S12. ^{1}H NMR spectrum of ligand **L** (in $CDCl_3$, top) and **Cage (**in CD_3CN, bottom).

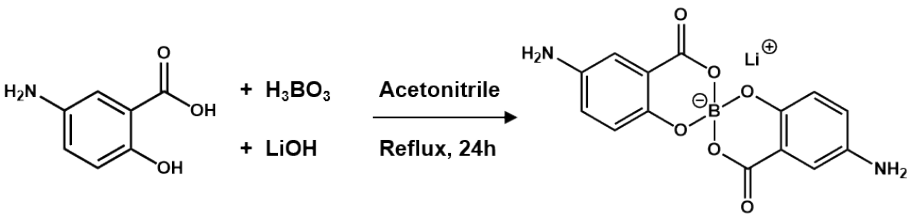

Figure S13. Synthesis diagram of LiB5AB.

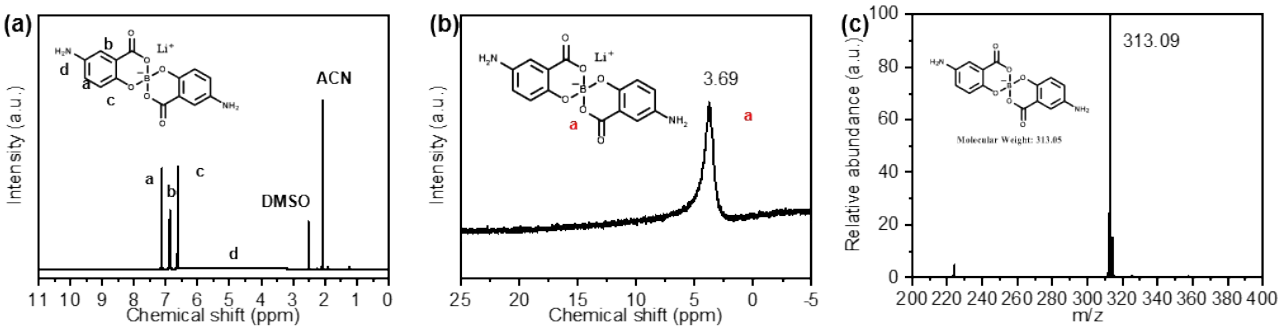

Figure S14. (a) ^{1}H NMR and (b) ^{11}B NMR spectra of LiB5AB. (c) Mass spectrum of LiB5AB.

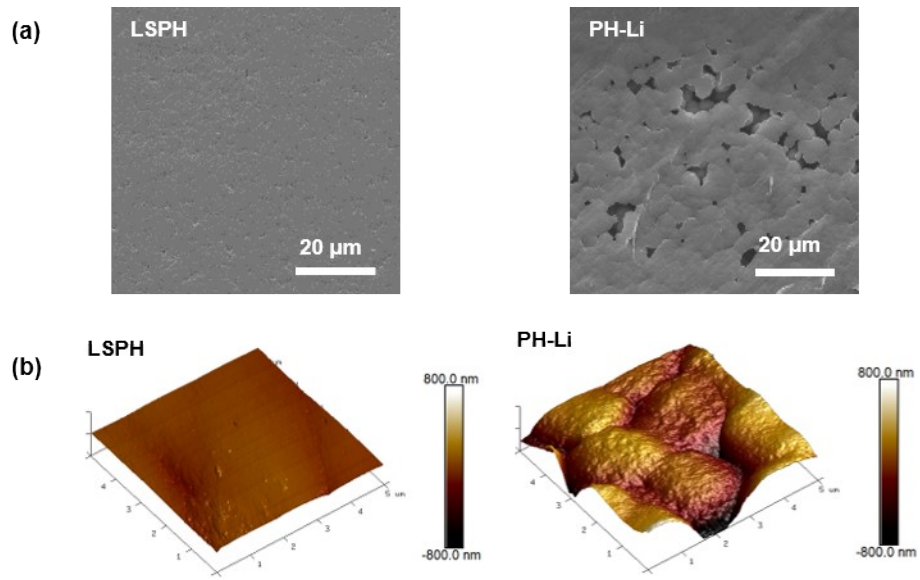

Figure S15. The (a) SEM images and (b) AFM images of LSPH (left) and PH-Li (right) electrolytes.

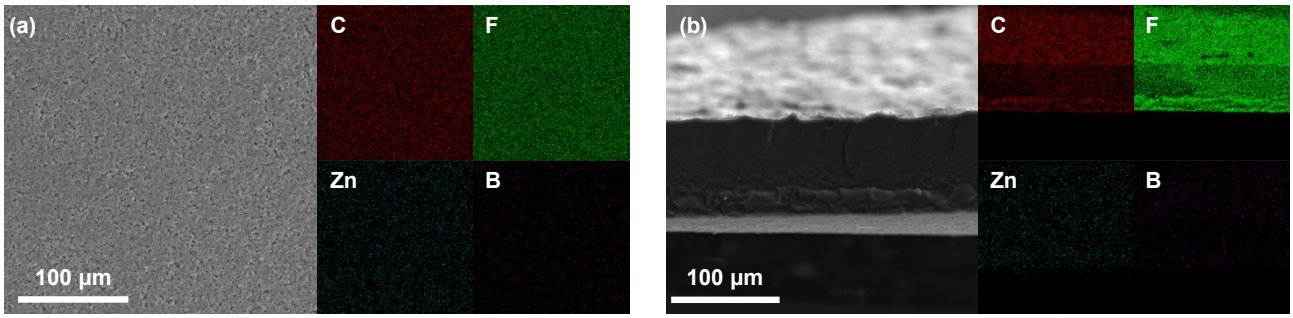

Figure S16. Surface (a) and cross-sectional (b) SEM images with corresponding EDS elemental mappings (C, F, Zn, and B) of the LSPH membrane.

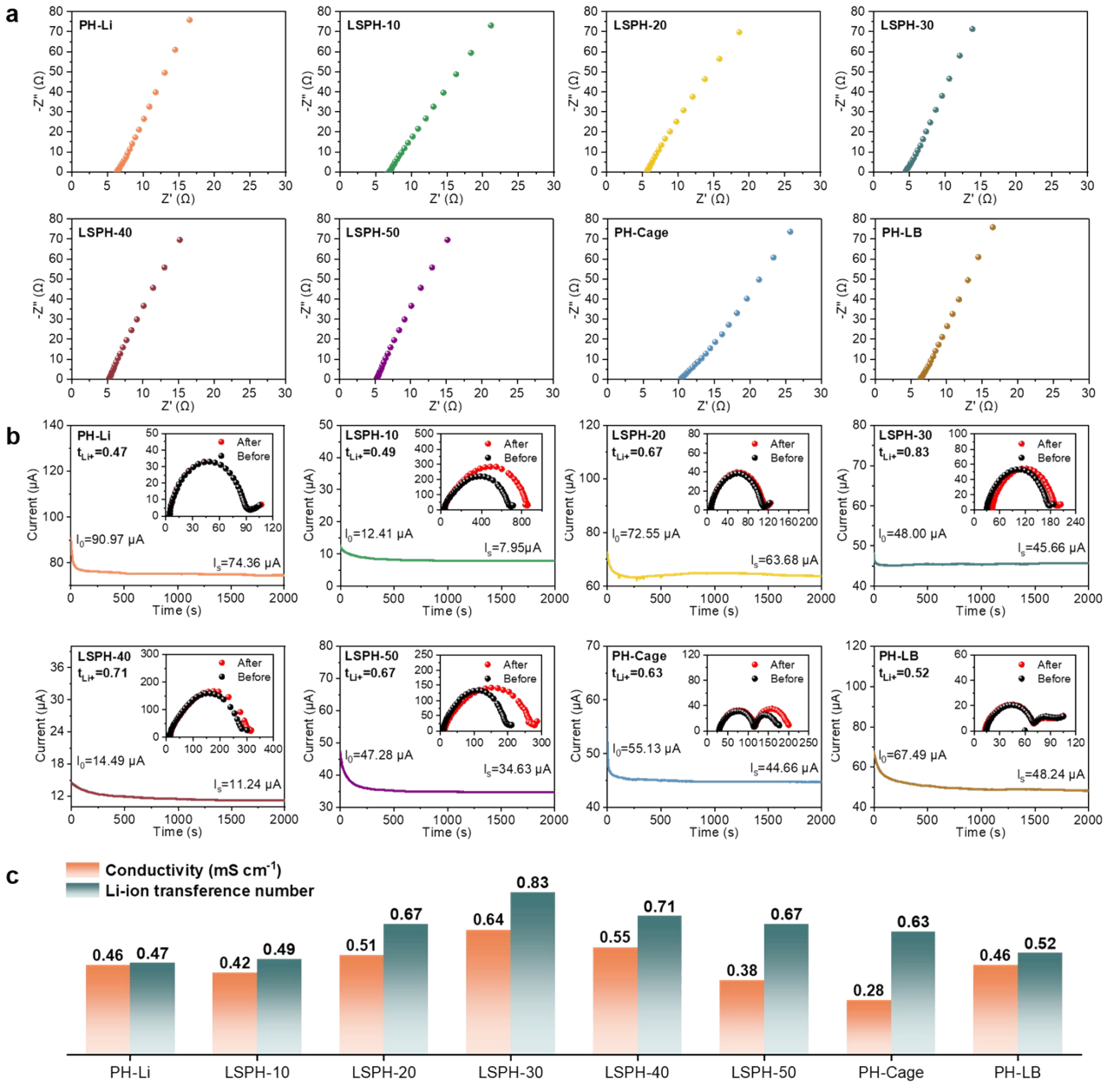

Figure S17. a) The EIS spectra of PH-Li, LSPH-10, LSPH-20, LSPH-30, LSPH-40, LSPH-50, PH-Cage and PH-LB electrolytes. b) Chronoamperometry profiles and AC impedance spectra before and after polarization (inset) for symmetric Li||Li cell with PH-Li, LSPH-10, LSPH-20, LSPH-30, LSPH-40, LSPH-50, PH-Cage and PH-LB electrolytes. c) Room-temperature ionic conductivity and Li-ion transference number of PH-Li, LSPH-10, LSPH-20, LSPH-30, LSPH-40, LSPH-50, PH-Cage and PH-LB electrolytes.

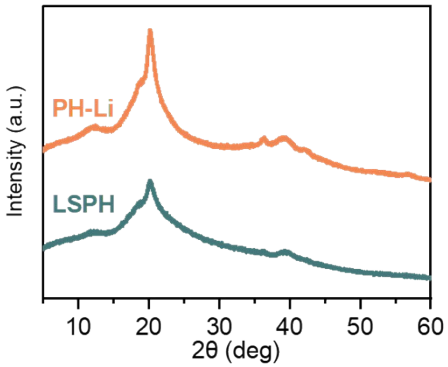

Figure S18. The XRD spectra of LSPH and PH-Li electrolytes.

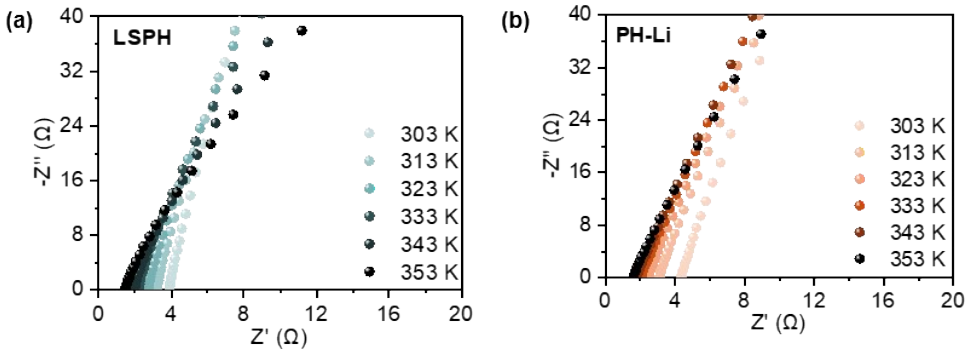

Figure S19. The EIS spectra of a) LSPH and b) PH-Li at different temperatures.

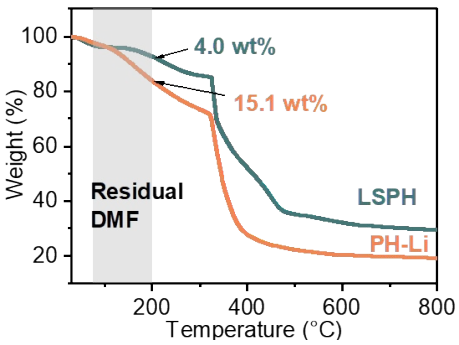

Figure S20. The TGA spectra of LSPH and PH-Li electrolytes.

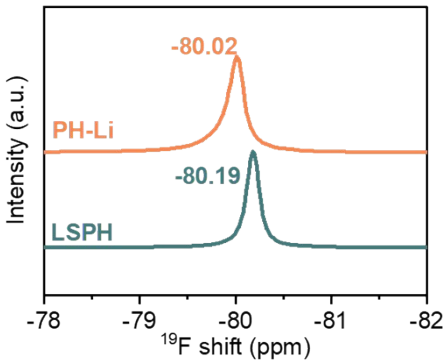

Figure S21. ^{19}F NMR spectra of LSPH and PH-Li.

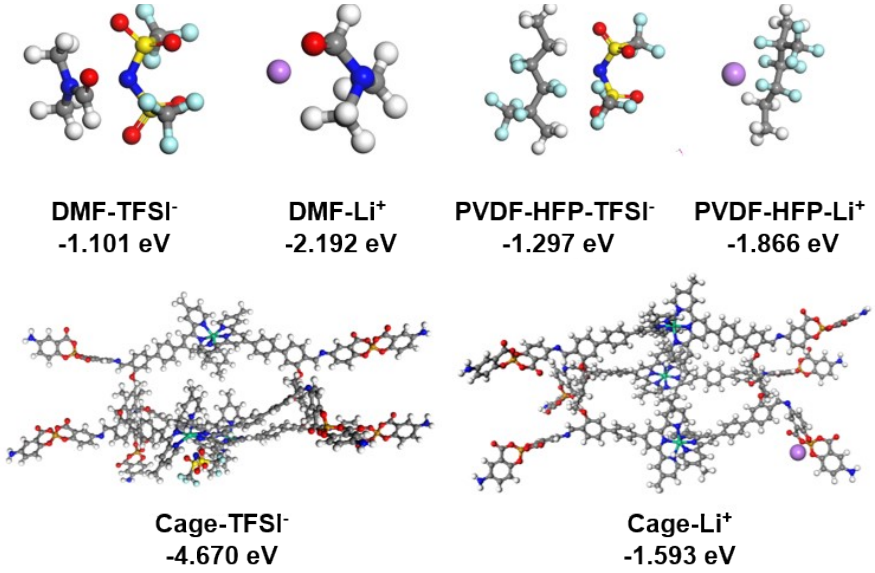

Figure S22. The coordination structures and the calculation of the binding energy for the molecular structures of PVDF-HFP, DMF and LS with Li^+ and $TFSI^-$, respectively.

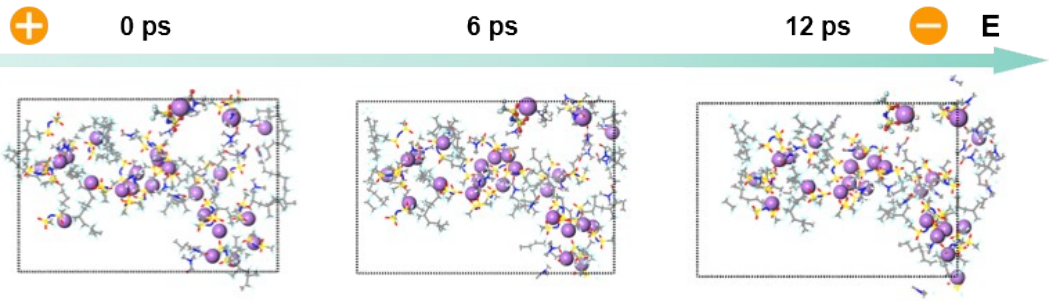

Figure S23. The migration model of Li^+, $TFSI^-$ and DMF in PH-Li under electric field.

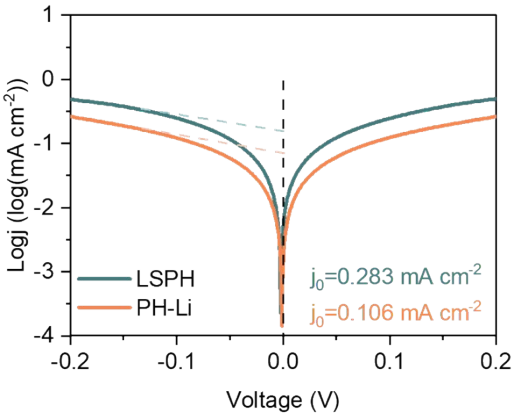

Figure S24. Tafel curves of Li||Li symmetric cells with LSPH and PH-Li electrolytes.

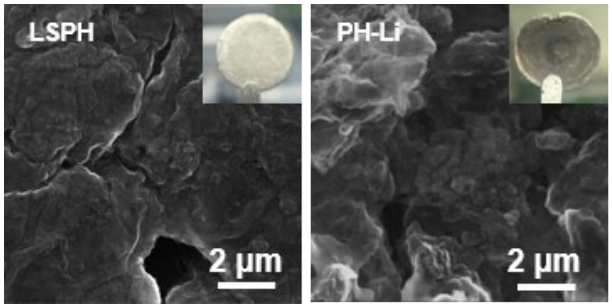

Figure S25. Top-view SEM images of Li metal electrode using LSPH and PH-Li electrolytes after 100 cycles at 1.0 mA cm^{-2}.

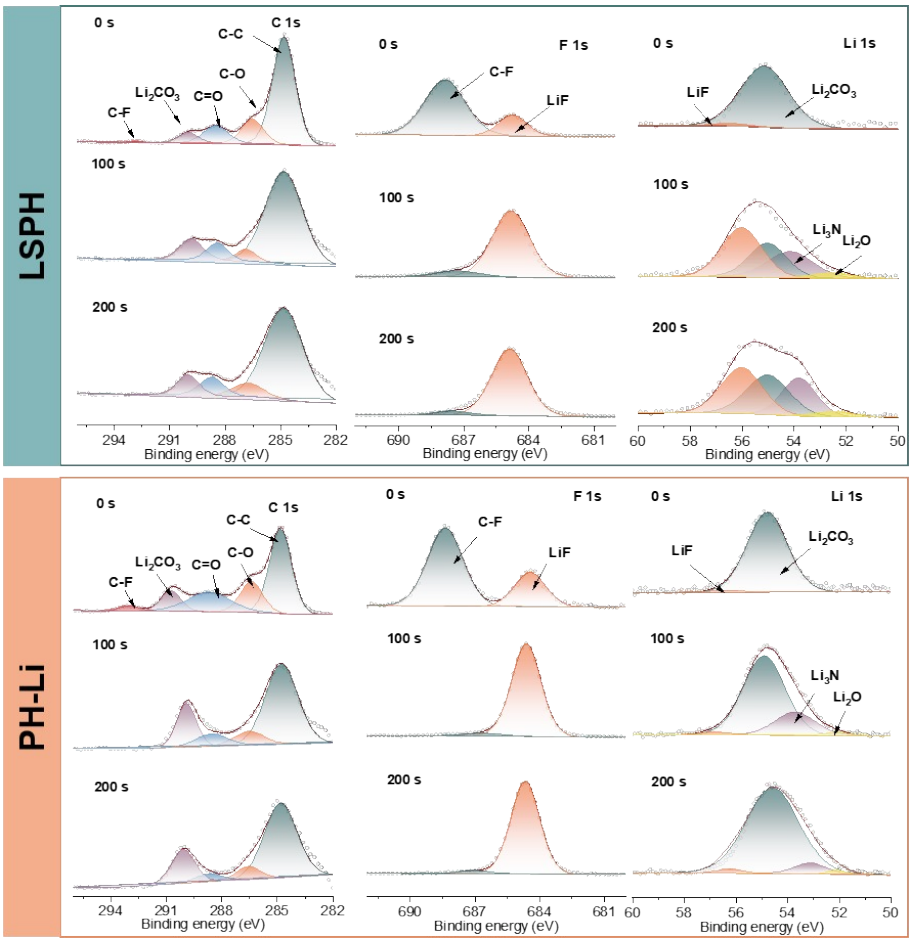

Figure S26. XPS spectra for C 1s, F 1s and Li 1s of the cycled Li metal anode in Li|LSPH|Li and Li|PH-Li|Li cell.

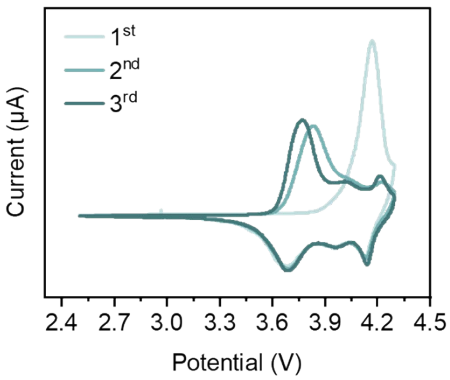

Figure S27. CV curve for Li|LSPH|NCM811 cell at 0.1 mV s^{-1}.

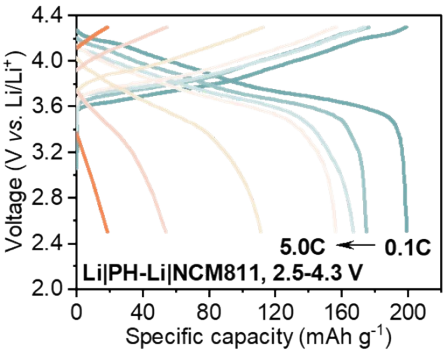

Figure S28. Charge/discharge profiles of Li|PH-Li|NCM811 cell at different rate.

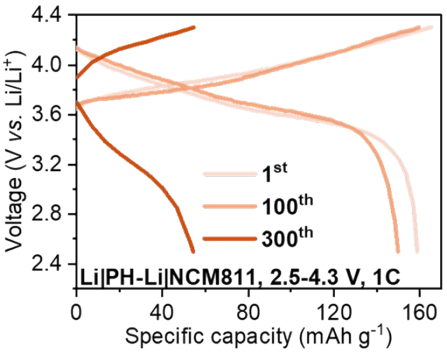

Figure S29. Charge/discharge profiles of Li|PH-Li|NCM811 cell at 1C.

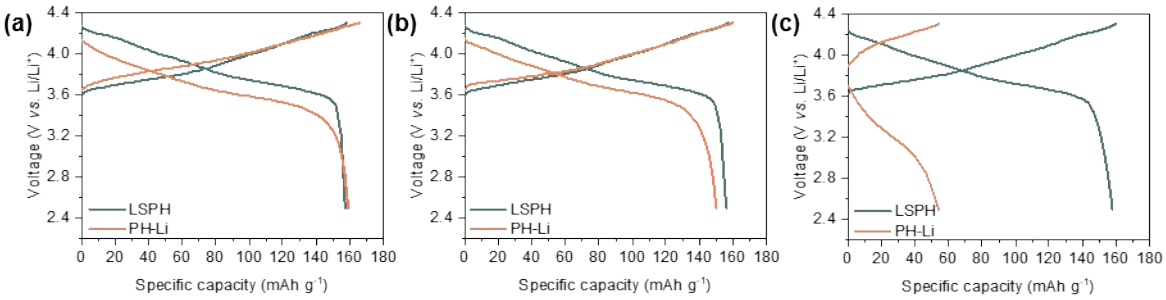

Figure S30. Comparison of charge-discharge profiles of Li||LSPH||NCM811 and Li||PH-Li||NCM811 full cells at 1.0 C (a) 1st cycle, (b) 100th cycle, and (c) 300th cycle.

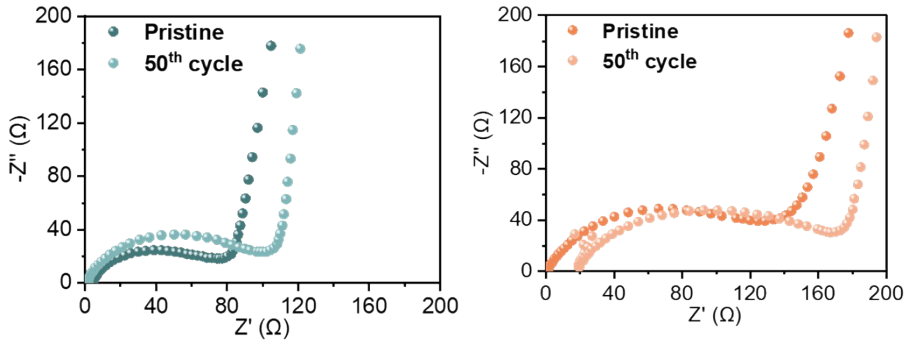

Figure S31. Electrochemical impedance measurements of the Li||NCM811 batteries with (a) LSPH and (b) PH-Li electrolytes, conducted before and after 50th cycle test.

Table S1. Comparison of Li|SPEs|Li batteries performance

Number	Electrolytes	Residual solvent content (wt.%)	Current density (mA cm^{-2})	Cycle time (h)	References
1	PVMS-15	12.46	1	480	*Nat. Commun.*, **2023**, 14, 6296
2	PVBL	14.4	1	300	*Nat. Nanotechnol.*, **2023**, 18, 602-610
3	HFGP-SE	22.7	0.5	1200	*Energy Environ. Sci.*, **2025**,18, 227-235
4	PPM	18.3	0.5	500	*Energy Environ. Sci.*, **2024**, 17, 8274-8283
5	BPLE-1	3.3	0.3	800	*Adv. Funct. Mater.*, **2025**, 2424763
6	LPS_x-5	4	1	400	*Adv. Mater.*, **2025**, 2419271
7	PV-MS20	17.1	0.5	240	*Angew. Chem. Int. Ed.*, **2024**, e202401428
8	CPS-6	3.4	0.5	800	*Angew. Chem. Int. Ed.*, **2025**, e202423227
9	F-PVDF	11.1	1	900	*Adv. Mater.*, **2025**, 2504419
10	d-PVDF SPE	17.65	0.3	275	*Energy Environ. Sci.*, **2024**, 17, 8243-8253
11	PTZN	9	0.2	1000	*Adv. Sci.*, **2025**, 12, 2413875
12	PLLDB	17	0.25	270	*J. Am. Chem. Soc.*, **2023**, 145, 25632-25642
This work	**LSPH**	**4**	**1**	**1000**	

Reference

1. G. Kresse and J. Furthmüller, *Comput. Mater. Sci.*, 1996, **6**, 15-50.
2. G. Kresse and J. Furthmuller, *Phys. Rev. B: Condens. Matter Mater. Phys.*, 1996, **54**, 11169-11186.
3. J. P. Perdew, K. Burke and M. Ernzerhof, *Phys. Rev. Lett.*, 1996, **77**, 3865-3868.
4. S. Grimme, J. Antony, S. Ehrlich and H. Krieg, *J. Chem. Phys.*, 2010, **132**, 154104.
5. H. J. Monkhorst and J. D. Pack, *Phys. Rev. B: Solid State*, 1976, **13**, 5188-5192.
6. W. G. Hoover, *Phys. Rev. A*, 1985, **31**, 1695-1697.
7. S. Nosé, *J. Chem. Phys.*, 1984, **81**, 511-519.
8. G. Wang, M. Chen, J. Wang, Z. Jiang, D. Liu, D. Lou, H. Zhao, K. Li, S. Li, T. Wu, Z. Jiang, X. Sun and P. Wang, *J. Am. Chem. Soc.*, 2020, **142**, 7690-7698.